AGU PUBLICATIONS

Geophysical Research Letters

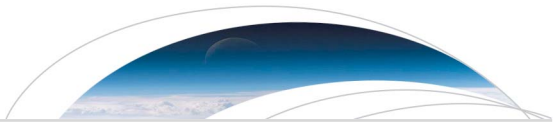

RESEARCH LETTER

10.1002/2015GL063186

Key Points:
- New geodetic and oceanographic estimates of the tilt of coastal mean sea level
- Cluster analysis shows convergence of the best estimates from both approaches
- Implications for understanding and projecting coastal sea level rise

Supporting Information:
- Readme
- Table S1

Correspondence to:
S. Higginson,
simon.higginson@dfo-mpo.gc.ca

Citation:
Higginson, S., K. R. Thompson, P. L. Woodworth, and C. W. Hughes (2015), The tilt of mean sea level along the east coast of North America, *Geophys. Res. Lett.*, *42*, 1471–1479, doi:10.1002/2015GL063186.

Received 20 JAN 2015
Accepted 2 FEB 2015
Accepted article online 5 FEB 2015
Published online 9 MAR 2015

The tilt of mean sea level along the east coast of North America

S. Higginson[1], K. R. Thompson[2], P. L. Woodworth[3], and C. W. Hughes[3,4]

[1]Bedford Institute of Oceanography, Dartmouth, Nova Scotia, Canada, [2]Department of Oceanography, Dalhousie University, Halifax, Nova Scotia, Canada, [3]National Oceanography Centre, Liverpool, UK, [4]School of Environmental Sciences, University of Liverpool, Liverpool, UK

Abstract The tilt of mean sea level along the North American east coast has been a subject of debate for many decades. Improvements in geoid and ocean circulation models, and GPS positioning of tide gauge benchmarks, provide an opportunity to produce new tilt estimates. Tilts estimated using tide gauge measurements referenced to high-resolution geoid models (the geodetic approach) and ocean circulation models (the ocean approach) are compared. The geodetic estimates are broadly similar, with tilts downward to the north through the Florida Straits and at Cape Hatteras. Estimates from the ocean approach show good agreement with the geodetic estimates, indicating a convergence of the two approaches and resolving the long standing debate as to the sign of the tilt. These tilts differ from those used by Yin and Goddard (2013) to support a link between changing ocean circulation and coastal sea level rise.

1. Introduction

There is a long history of attempts to measure the tilt of mean sea level along the east coast of North America and to relate it to the circulation of the adjacent shelf and deep ocean [e.g., *Bowie*, 1927; *Montgomery*, 1938; *Sturges*, 1974; *Scott and Csanady*, 1976; *Sturges*, 1977; *Csanady*, 1978; *Chapman et al.*, 1986; *Lentz*, 2008; *Xu and Oey*, 2011]. *Bowie* [1927] used geodetic leveling surveys to argue that coastal mean sea level tilted upward toward the north and suggested a link to meteorological conditions and ocean density variations. *Montgomery* [1938] used the difference in mean sea level between tide gauges on the east and west coasts of Florida, linked by leveling, to estimate the mean speed of the Florida Current. He assumed that a loss of potential energy was balanced by a gain of kinetic energy but concluded that the method did not produce reasonable results. *Sturges* [1974] proposed that a tilt exists along the inshore edge of the Gulf Stream from Florida to Cape Hatteras related to the variation of the Coriolis parameter with latitude.

Using a simple across-stream geostrophic balance and measurements of the Gulf Stream surface transport and cross-stream gradient, *Sturges* [1974] estimated a tilt of 2.0 ± 0.4 cm/degree latitude (equivalent to a tilt of 2.2×10^{-7}) downward from Florida to Cape Hatteras. This tilt was in good agreement with estimates from steric height calculations but in the opposite direction to estimates from geodetic leveling. *Fischer* [1977] attempted to reconcile this difference between geodetic and oceanographic estimates by comparing the reference surfaces and terminologies of the two disciplines.

In the Middle Atlantic Bight (MAB), a number of oceanographic studies have estimated an alongshore pressure gradient and concluded it tilts down toward the south. For example, *Scott and Csanady* [1976] estimated a tilt of 1.44×10^{-7} (equivalent to 1.44 cm per 100 km) while *Lentz* [2008] estimated a tilt of 0.37×10^{-7} north of Chesapeake Bay (37°N) and zero to the south. However, there has been a disagreement whether this pressure gradient originates offshore or on the shelf [e.g., *Csanady*, 1978; *Chapman et al.*, 1986; *Xu and Oey*, 2011].

It has proven difficult to measure the alongshore tilt of sea level at the coast because errors in geodetic leveling are large compared to the magnitude of the tilt. For example, *Sturges* [1977] suggested that leveling errors may exceed the tilt of order 10^{-7} determined oceanographically by *Scott and Csanady* [1976]. Satellite gravity missions in the last 15 years have contributed to geoid model improvements, bringing geoid accuracy to the centimeter level [e.g., *Bingham et al.*, 2011]. With these improvements, and GPS positioning of tide gauges, it is feasible to observe these tilts directly from coastal tide gauge data. *Woodworth et al.* [2012, hereafter W12], examined tilts along the coastlines of the eastern and western Atlantic and the eastern Pacific. They found broadly comparable results by referencing tide gauge

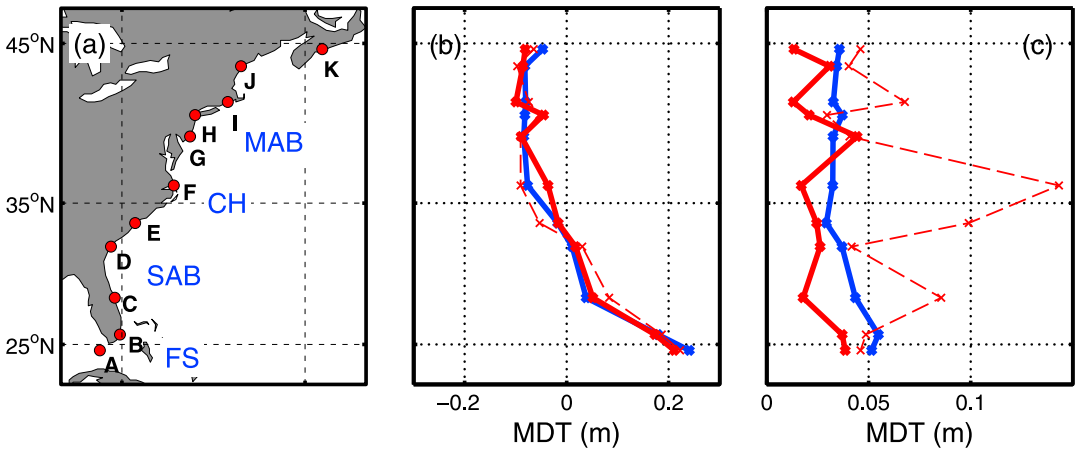

Figure 1. (a) The location of the tide gauges. (A: Key West, B: Virginia Key, C: Trident Pier, D: Savannah, E: Springmaid Pier, F: Duck, G: Atlantic City, H: New York, I: Newport, J: Portland, and K: Halifax.) The main geographic features mentioned in the text are shown in blue (FS: Florida Straits, SAB: South Atlantic Bight, CH: Cape Hatteras, and MAB: Middle Atlantic Bight.) (b) The mean MDT estimate from all geoid models (red dashed line), the first cluster of geoid models (red solid line), and from all ocean models (blue line). (c) Same as Figure 1b but showing the standard deviation of the model estimates. The spatial mean of each profile was removed before analysis.

measurements of mean sea level to the geoid (the "geodetic" approach) and using ocean circulation models (the "ocean" approach). Comparing estimates from one geoid model and one ocean model, they found that the standard deviation of differences was 9.5 cm along the east coast of North America.

Although the observed alongshore tilts are typically small compared to sea level gradients in the deep ocean, W12 showed a number of locations within their study area where relatively large tilts exist. Two of the most prominent are in the Florida Straits and at Cape Hatteras, both regions where the Gulf Stream passes close to the coastline, although there are considerable differences in the magnitude of the tilts between different estimates. For example, their estimates from the ocean approach around Cape Hatteras (between Springmaid Pier and Duck tide gauges, E and F in Figure 1a) range from 1.1×10^{-7} upward to the north to 3.2×10^{-7} downward.

There has been recent interest in sea level along the East Coast of the U.S., and in the area north of Cape Hatteras, in particular, because of the identification of a sea level rise acceleration "hot spot" since the 1980s [e.g., *Sallenger et al.*, 2012; *Boon*, 2012]. It has been proposed that coastal sea level variability in this region is related to the Gulf Stream and the Atlantic meridional overturning circulation [e.g., *Bingham and Hughes*, 2009; *Ezer et al.*, 2013]. *Yin and Goddard* [2013] used satellite altimeter measurements to identify a pronounced alongshore tilt in mean coastal sea level north of Cape Hatteras, downward to the north. They proposed that this is related to the alongshore change in the across-Gulf Stream sea level gradient and is consistent with a correlation between a decline in the Gulf Stream strength and the acceleration of coastal sea level rise over the last 20 years. However *Andres et al.* [2013] found that the interannual variability of sea level along the shelf in this region is strongly correlated with local wind forcing, and *Rossby et al.* [2014] used in situ measurements to show that there has been no change to the strength of the Gulf Stream downstream (northward) of Cape Hatteras over the period of sea level rise acceleration.

In this study we compare new estimates of the tilt of mean sea level along the western boundary of the North Atlantic obtained using the geodetic and ocean approaches. We show a convergence of the two approaches and propose dynamical explanations for the observed tilts. From a climate change and coastal flooding perspective it is essential that models correctly represent processes affecting sea level at the coast. This study adds to our knowledge of how the coast "sees" changes in the deep ocean and thereby contributes to our understanding of links between the ocean circulation and coastal sea level rise. From an ocean modeling perspective, measurements of the alongshore tilts of sea level are potentially useful for model validation. This study is a natural extension of earlier comparisons of the geodetic and ocean approaches in the deep ocean [e.g., *Bingham and Haines*, 2006; *Higginson et al.*, 2011; *Griesel et al.*, 2012] and complements studies of apparent alongshore slopes in Australia [*Featherstone and Filmer*, 2012; *Filmer*, 2014]

and Great Britain [*Penna et al.*, 2013]. It builds on the comparisons presented by W12, using quantitative approaches to demonstrate, and physically explain, the convergence of the two approaches.

The structure of the paper is as follows. In section 2 we describe the geodetic and oceanic estimates of the alongshore tilt of mean sea level along the east coast of North America, and in section 3 we describe a quantitative comparison of the tilts. Dynamical explanations for the main features of the tilts are proposed in section 4, and in section 5 the new contributions from this study are discussed.

2. Estimates of the Alongshore Tilt of Coastal Mean Sea Level

The geodetic approach is based on the difference between mean sea level observed at coastal tide gauges and the height of the geoid, with both heights expressed relative to the same reference ellipsoid. The ocean approach is based on the mean sea surface height at coastal points that are calculated using an ocean circulation model. While absolute values may differ, depending on the model, this study focuses on the tilts, which should be comparable.

2.1. Geodetic Approach

Monthly tide gauge data were obtained from the Revised Local Reference (RLR) data set of the Permanent Service for Mean Sea Level (PSMSL) [*Woodworth and Player*, 2003], with mean sea level (MSL) at each location referenced to a local benchmark. GPS ellipsoidal heights at these benchmarks, or nearby benchmarks connected to the tide gauge benchmarks by leveling, were obtained from the shared solutions of the National Geodetic Survey's Online Positioning User Service (OPUS) (http://www.ngs.noaa.gov/OPUS) for U.S. stations and from Natural Resources Canada (http://webapp.geod.nrcan.gc.ca/geod/data-donnees/passive-passif.php) for Canadian stations. OPUS ellipsoid heights were obtained from GPS occupations of at least 4 h, processed using nearby continuously operating GPS stations to give vertical accuracies of better than $\pm$1 cm except at Atlantic City ($\pm$2.5 cm), Springmaid Pier ($\pm$1.1 cm) and Savannah ($\pm$2.2 cm). The heights were converted to International Terrestrial Reference Frame (ITRF) 2008, epoch 2010.0 [*Altamimi et al.*, 2011], using the Horizontal Time-Dependent Positioning utility [*Pearson and Snay*, 2013]. The MSL RLR values were converted to MSL relative to the GRS80 ellipsoid using these benchmark ellipsoidal heights, with all values expressed in tide-free form using permanent tide conversions in accordance with *Ekman* [1989]. An inverse barometer adjustment was applied using a reference air pressure of 1013.3 mbar, as described by W12, to provide compatibility with the ocean approach. Tide gauge locations were chosen where the record is near complete (at least 90% of monthly means are available) for the period 1996 to 2000, and where (for U.S. stations) an OPUS-processed tidal benchmark is available within 1 km. We expect the error contributed by leveling over these distances to be negligible. Eleven locations were chosen to provide a relatively uniform distribution along the coastline of North America (Figure 1a), although results similar to those presented were obtained using different combinations of gauges.

The mean dynamic topography (MDT) was calculated by subtracting the geoid height from the ellipsoidal MSL using seven recent geoid models (Table 1). Each model was adjusted to ITRF 2008 and expressed in the tide-free system. Figures 1b and 1c (red dashed lines) show the mean and standard deviation of the MDT estimates (in m) after the spatial mean MDT for each profile was removed. The highest MDT values are observed in southern Florida, with a drop of approximately 20 cm toward northern Florida and a smaller drop near Cape Hatteras.

2.2. Ocean Approach

MDT was estimated at the same tide gauge locations using 11 ocean circulation models (Table 1), differing in their horizontal resolution and whether hydrographic and sea level observations had been assimilated. The models include those used by W12, although we exclude models with a relatively coarse 1° horizontal resolution. Where models are not available for the same time period as the geodetic approach estimates, values are adjusted by the difference between the tide gauge MSL for the model period and the 1996–2000 period. MDT is calculated using the model's wet grid cell nearest to each tide gauge location. Figures 1b and 1c show the mean and standard deviation of the MDT estimates, with the spatial mean MDT for each profile removed in the same way as for the geodetic approach estimates. The highest MDT values are observed in southern Florida, similar to the geodetic approach estimates, with drops toward northern Florida and near Cape Hatteras.

Table 1. The Geoid and Ocean Models

Code	Model Name	Time Period	Degree/Order or Grid Spacing	Data[a]	Reference and/or Source
Geoid					
G1	CGG2013		2 arc min	s,t	*Huang and Veronneau* [2013] (webapp.geod.nrcan.gc.ca)
G2	EGM2008		2190	s,t	*Pavlis et al.* [2012]
G3	GOCO03S		250	s	www.goco.eu/
G4	USGG2012		1 arc min	s,t	www.ngs.noaa.gov/GEOID
G5	GGMplus		7.2 arc sec	s,t	*Hirt et al.* [2013] (geodesy.curtin.edu.au/research/)
G6	TUM2013C		720	s,t	*Fecher et al.* [2013]
G7	GOCO03S extended		2190	s,t	*Woodworth et al.* [2012]
Ocean					
O1	ECCO2	1996–2000	18 km	T,S,η	*Menemenlis et al.* [2008] (ecco2.jpl.nasa.gov/)
O2	OCCAM	1996–2000	1/12°	-	*Marsh et al.* [2009]
O3	Liverpool	1996–2000	1/6°	T,S	*Woodworth et al.* [2012]
O4	NOC ORCA12	1996–2000	1/12°	-	*Duchez et al.* [2014]
O5	HYCOM	1996–2000	1/12°	T,S,η	*Chassignet et al.* [2009] (hycom.org/)
O6	HYCOM	2003–2006	1/12°	-	*Chassignet et al.* [2009] (hycom.org/)
O7	Mercator	2013	1/12°	T,S,η	www.myOcean.eu
O8	Glorys2v3	1996–2000	1/4°	T,S,η	www.myOcean.eu
O9	UR025	1996–2000	1/4°	T,S,η	www.myOcean.eu
O10	CGLORS	1996–2000	1/4°	T,S,η	www.myOcean.eu
O11	MJM105b	1996–2000	1/4°	-	www.myOcean.eu

[a]For the geoid models, the data sources are s (satellite) and t (terrestrial). For the ocean models the data assimilated are T (temperature), S (salinity), and η (sea surface height).

3. Comparison of Geodetic and Ocean Estimates

The mean alongshore profiles from the geodetic and ocean approaches are remarkably similar (dashed red and blue lines in Figure 1b), with a standard deviation of differences of 2.3 cm. However, the variability is much higher among the individual geodetic estimates than the ocean estimates (Figure 1c, average standard deviations 6.3 cm and 3.8 cm, respectively.) To identify groups of profiles with lower variability we undertook independent cluster analysis of the geodetic profiles and compared the clusters with the ocean estimates.

The *k*-means method [e.g., *Jain*, 2010] was used to cluster the profiles. This method partitions *m* multivariate observations into *k* clusters by iteratively minimizing the sum, over all clusters, of the within-cluster sums of observation-to-centroid squared distances. For each cluster the centroid is the mean of the cluster's members, and distance is the Euclidean distance between a cluster member and the centroid.

There are $m = 7$ geoid models, each providing MDT estimates at the 11 tide gauge locations. We used the gap statistic [*Tibshirani et al.*, 2001] to estimate the appropriate number of clusters and found $k = 2$. The first cluster (hereafter GC1) includes all of the geoid models except GOCO03S. The variability of the profiles is considerably less when GOCO03S is excluded (Figure 1c, average standard deviation 2.6 cm.) This variability can be considered an estimate of the error in the geoid models. The mean GC1 profile is in good agreement with the mean profile from the ocean approach (Figure 1b). There is a drop of about 20 cm between southern and northern Florida (a tilt of 3.5×10^{-7}) and a smaller drop around Cape Hatteras (less than

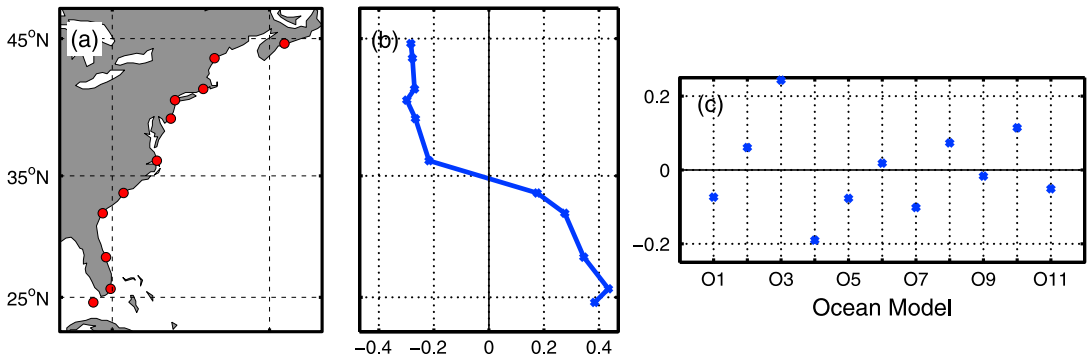

Figure 2. Summary of the variability of the ocean model profiles based on a covariance-based principal component analysis. (a) The location of the tide gauges. (b) The first mode, representing 84% of the variability. The mode (first eigenvector) has been normalized to have unit length. (c) The amplitude (in m) of the first mode for each of the ocean models.

1×10^{-7}). In the MAB the profiles are nearly flat. However, there is a slight rise to the north at the three tide gauges north of New York, which is in agreement with tilt estimates on the shelf [e.g., *Lentz*, 2008].

Applying the gap statistic to the ocean estimates showed there to be only one cluster. However, there is spatially structured variability within the cluster. From a principal component analysis based on the covariance matrix, we found the first spatial mode (Figure 2b). This mode accounts for 84% of the variability of the ocean profiles about the mean shown in Figure 1b. The mode describes large variations in the tilt at Cape Hatteras, embedded within a weaker, but large scale, tilt of the same sign over most of the study area. The amplitude of the dominant mode (Figure 2c) describes the individual contributions of this mode to each model profile. Intermodel differences in the drop at Cape Hatteras range between an increase of about 9 cm (O3) and a decrease of about 8 cm (O4) relative to the mean (Figure 1b, blue line).

4. A Dynamical Interpretation

The surface circulation of the western North Atlantic is dominated by the Gulf Stream system. As the Florida Current passes through the Florida Straits, it follows the narrow shelf and passes within 20 km of the shore [e.g., *Leaman et al.*, 1987]. The shelf widens as the current flows north and it follows the shelf break which is typically more than 100 km from shore in the South Atlantic Bight (SAB). The mean near-coast currents flow northward but are considerably weaker and more variable than the Florida Current offshore [e.g., *Atkinson et al.*, 1983]. At Cape Hatteras the Gulf Stream leaves the shelf break and heads offshore. North of Cape Hatteras the flow on the shelf from the Scotian Shelf to the Mid-Atlantic Bight (MAB) is generally to the southwest. Near Cape Hatteras this flow is incorporated into the Gulf Stream and moves offshore [e.g., *Xu and Oey*, 2011].

Most of these circulation features are evident in Figure 3 (left), which shows a contour map of MDT from the HYCOM data-assimilating ocean circulation model. (This model is reference O5 in Table 1 and is one of the ocean models in closest agreement with the geodetic estimate of coastal tilt.) For example, the Florida Current can be seen close to shore near Miami, moving offshore as it follows the shelf break northward toward Cape Hatteras. Sea level differences of order 1 m mark the path of the Gulf Stream as it moves into deep water. North of Cape Hatteras the model MDT at the shelf break is generally lower than at the coast, consistent with a geostrophically balanced surface flow toward the southwest.

The variation of model MDT along the 2000 m and 200 m depth contours, and along the coast, are plotted in Figure 3 (right). The 2000 m and 200 m isobaths were chosen to characterize the MDT signal in the deep ocean and along the shelf break, respectively. The deep ocean tilt is dominated by the drop of approximately 1 m across the Gulf Stream as it moves offshore and crosses the 2000 m isobath. The coastal profile shows a downward tilt through the Florida Straits, a sharp drop onto the SAB shelf and a slight downward tilt toward Cape Hatteras. However, there is no pronounced drop at Cape Hatteras where the Gulf Stream moves offshore, as is seen in the deep ocean tilt. The shelf break profile corresponds with the coastal tilt through the Florida Straits, but MDT continues to fall more gradually toward Cape Hatteras, and there is a drop of order 20 cm where the Gulf Stream separates at Cape Hatteras.

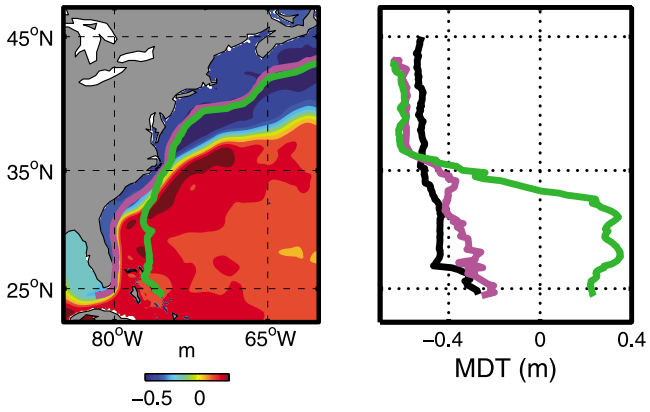

Figure 3. MDT from the HYCOM data-assimilative ocean model (Table 1, reference O5). (left) MDT (in m) from the model. The magenta and green lines show the smoothed location of the 200 m and 2000 m isobaths, respectively. (right) MDT along the coastline (black) and along the 200 m (magenta) and 2000 m (green) isobaths, plotted against latitude.

A number of studies have examined deep ocean forcing of the circulation on the adjacent slope and shelf (*Huthnance* [1992] provides a comprehensive review). For example, *Csanady* [1982] used "arrested topographic wave" theory (based on the assumption of linear, steady, depth-averaged, and barotropic flow on an *f* plane) to obtain an explicit expression for sea level at the coast given sea level along an offshore boundary. He showed that relatively long wavelength variability at the boundary is detected at the coast with little attenuation, but short wavelength variability does not penetrate across the shelf. *Wright* [1986] and *Middleton* [1987] showed that the propagation of a deep ocean pressure gradient may be influenced by the width and steepness of the shelf. *Huthnance* [2004] used a more sophisticated baroclinic model with a three-dimensional representation of the flow to conclude that coastal sea level only responds to ocean forcing with long length scales (typically thousands of kilometers).

Coastal MDT from Figure 3 (right) shows little or no tilt throughout the SAB and the MAB, consistent with *Csanady* [1982] and *Huthnance* [2004]. However, there is a tilt of coastal MDT through the Florida Straits. To understand this tilt, we assume a steady state with no flow normal to the coast and take the alongshore momentum balance at the coast to be

$$g\frac{\partial \eta}{\partial y} = F_y - \frac{1}{2}\frac{\partial}{\partial y}|v|^2 \tag{1}$$

where g is acceleration due to gravity, v is the depth-averaged alongshore flow, and F_y denotes the combined effect of lateral and bottom friction and wind stress. Note that the steric term is omitted because the water depth tends to zero at the coast, and the geostrophic contribution is omitted because of the assumption of no normal flow. *Montgomery* [1938] considered a balance between the first and third terms, but scaling shows this balance to account for a relatively small tilt. (For example, an alongshore speed difference of 50 cm s^{-1} at the coast is balanced by a sea level difference of 1.25 cm.) Considering only the first and second terms, the bottom and lateral friction are generally larger where the flow is faster, and these forces are balanced by the tilt. In the Florida Straits the shelf is narrow, the Florida Current passes close to shore, leading to reduced attenuation of the deep ocean signal, consistent with the tilt of coastal MDT balancing the frictional forces. Further north, in the SAB, the same simple balance accounts for the (small) tilt along the coast, related to the (weak) alongshore flow, with the shelf partially insulating the coast from the deep ocean signal.

At Cape Hatteras the models in GC1 produce a small (or no) alongshore tilt. Some of the ocean models show a similar tilt, while others have a drop of 15 cm (see Figure 2c for the contribution of the first mode to the tilt for each model). One explanation for these differences is that some ocean models do not accurately represent the processes operating in the shallow waters near the coast. This could result in the models detecting the shelf break tilt at the coast. As seen from the magenta and black lines in Figure 3 (right), this would lead to coastal sea level estimates that are too high south of Hatteras, and too low to the north. Alternative explanations include inadequate horizontal resolution to represent the shelf bathymetry,

the form of the coastal boundary condition, and incorrect atmospheric forcing or boundary conditions (including freshwater inputs at the coast). W12 include a discussion of these limitations of global ocean models for reproducing sea level at the coast.

5. Summary and Discussion

Recent improvements in geoid modeling and GPS positioning of tide gauge benchmarks have made it possible to estimate the alongshore tilt of mean sea level with unprecedented accuracy, as shown by W12.

In this study we have built on the work of W12 by means of a more detailed analysis of the tilts along the east coast of North America, an area with a long history of attempts to measure the tilts. Using a clustering technique we show an encouraging level of agreement between a group of estimates from the geodetic approach and the ocean approach. These estimates show a mean tilt of 3.5×10^{-7} downward from the Florida Keys to Cape Canaveral and a much smaller (or no) tilt at Cape Hatteras. (The overall tilt is similar to estimates by *Sturges* [1974], but he considered a uniform tilt over the region.) The geodetic estimates (GC1) are from recent geoid models derived from satellite and terrestrial gravity measurements, including the CGG2013 model, an early version of which has been validated against oceanographic measurements offshore [*Higginson et al.*, 2011]. The agreement of the two mean profiles indicates a convergence of the geodetic and ocean approaches. This is similar to the convergence that has been described in the deep ocean previously [e.g., *Bingham and Haines*, 2006], using satellite altimeter measurements in place of tide gauge heights. The coastal convergence also provides valuable verification of geoid models in terms of worldwide height system unification.

While the mean profiles show good agreement, there is considerable variability among the ocean profiles in terms of the tilt at Cape Hatteras. Model resolution and data assimilation may partly explain the differences but, for example, the data assimilative 1/4° GLORYS2v3 (code O8) produces too steep a tilt (indicated by a positive amplitude in Figure 2c), whereas the free run MJM105b (code O11) does not. A more in-depth investigation is required using high-resolution ocean models and sensitivity studies involving, for example, different spatial resolution, frictional parameterizations, lateral boundary conditions, and external forcing.

Several recent studies have suggested that sea level acceleration north of Cape Hatteras can be attributed to changes in the Gulf Stream. Clearly, it is important to understand linkages between the deep ocean and coastal sea level to be able to make coastal flooding projections under different climate change scenarios. *Yin and Goddard* [2013] estimated coastal tilts of mean sea level using a satellite altimeter product and an ocean model, and showed a correlation between these patterns and the sea level gradient across the Gulf Stream. They suggested that a decrease in the speed of the Gulf Stream, and hence the cross-stream sea level gradient, leads to a rise of coastal sea level. However, their tilt estimates, downward from Cape Hatteras to 40°N, are approximately 9×10^{-7} and 6×10^{-7} (altimeter and model respectively), compared with less than 2×10^{-7} from GC1. Both the altimeter product and the ocean model they used were defined on a relatively coarse 1° horizontal grid, and it seems likely that their coastal estimates are more representative of the offshore region. We have shown that offshore mean sea level is only likely to be representative of the coastal signal in areas where the shelf is narrow, such as the Florida Straits, suggesting that these products cannot be used to support a link between changing ocean circulation and coastal sea level in the hot spot region. More generally, a number of ocean models produce mean sea level gradients around Cape Hatteras that do not agree with the geodetic approach estimates, and this may have implications for sea level rise projections in the hot spot. Our study illustrates that the relationship between the deep ocean and coastal sea level is complex. This relationship varies along the coastline because of differences in shelf geometry, and accurate estimation of coastal sea level will likely require high-resolution modeling to downscale deep ocean sea level features.

Acknowledgments

We thank Thomas Gruber, Technical University of Munich, for providing geoid model data and other assistance. This study has been conducted using MyOcean products. Data supporting Figures 1 and 2 are available in the supporting information Table S1. K.R.T. acknowledges support from the NSERC Discovery Grant Program and from the MEOPAR Network, funded by the Government of Canada's Networks of Centres of Excellence Program. Part of this work was cofunded by the European Space Agency and the UK Natural Environment Research Council.

The Editor thanks two anonymous reviewers for their assistance in evaluating this paper.

References

Altamimi, Z., X. Collilieux, and L. Métivier (2011), ITRF2008: An improved solution of the International Terrestrial Reference Frame, *J. Geod.*, *85*(8), 457–473, doi:10.1007/s00190-011-0444-4.

Andres, M., G. G. Gawarkiewicz, and J. M. Toole (2013), Interannual sea level variability in the western North Atlantic: Regional forcing and remote response, *Geophys. Res. Lett.*, *40*, 5915–5919, doi:10.1002/2013GL058013.

Atkinson, L., J. Blanton, W. Chandler, and T. Lee (1983), Climatology of the southeastern United States continental shelf waters, *J. Geophys. Res.*, *88*, 4705–4718.

Bingham, R., and K. Haines (2006), Mean dynamic topography: Intercomparisons and errors, *Phil. Trans. R. Soc. A*, *364*(1841), 903–916, doi:10.1098/rsta.2006.1745.

Bingham, R., and C. Hughes (2009), Signature of the Atlantic meridional overturning circulation in sea level along the east coast of North America, *Geophys. Res. Lett.*, *36*, L02603, doi:10.1029/2008GL036215.
Bingham, R. J., P. Knudsen, O. Andersen, and R. Pail (2011), An initial estimate of the North Atlantic steady-state geostrophic circulation from GOCE, *Geophys. Res. Lett.*, *38*, L01606, doi:10.1029/2010GL045633.
Boon, J. D. (2012), Evidence of sea level acceleration at U.S. and Canadian tide stations, Atlantic coast, North America, *J. Coastal Res.*, *28* (6), 1437–1445, doi:10.2112/JCOASTRES-D-12-00102.1.
Bowie, W. (1927), Tilting of mean sea level, *Gerlands Beitraege zur Geophysik*, *23*, 97–98.
Chapman, D. C., J. A. Barth, R. C. Beardsley, and R. G. Fairbanks (1986), On the continuity of mean flow between the Scotian Shelf and the Middle Atlantic Bight, *J. Phys. Oceanogr.*, *16*(4), 758–772, doi:10.1175/1520-0485(1986).
Chassignet, E., et al. (2009), U.S. GODAE: Global ocean prediction with the HYbrid Coordinate Ocean Model (HYCOM), *Oceanography*, *22*, 65–75.
Csanady, G. T. (1978), The arrested topographic wave, *J. Phys. Oceanogr.*, *8*(1), 47–62, doi:10.1175/1520-0485(1978)008.
Csanady, G. T. (1982), *Circulation in the Coastal Ocean*, 279 pp., D. Reidel, Netherlands.
Duchez, A., E. Frajka-Williams, N. Castro, J. Hirschi, and A. Coward (2014), Seasonal to interannual variability in density around the Canary Islands and their influence on the Atlantic meridional overturning circulation at 26°N, *J. Geophys. Res. Oceans*, *119*, 1843–1860, doi:10.1002/2013JC009416.
Ekman, M. (1989), Impacts of geodynamic phenomena on systems for height and gravity, *J. Geod.*, *63*, 281–296, doi:10.1007/BF02520477.
Ezer, T., L. P. Atkinson, W. B. Corlett, and J. L. Blanco (2013), Gulf Stream's induced sea level rise and variability along the U.S. mid-Atlantic coast, *J. Geophys. Res. Oceans*, *118*, 685–697, doi:10.1002/jgrc.20091.
Featherstone, W. E., and M. S. Filmer (2012), The north-south tilt in the Australian Height Datum is explained by the ocean's mean dynamic topography, *J. Geophys. Res.*, *117*, C08035, doi:10.1029/2012JC007974.
Fecher, T., R. Pail, and T. Gruber (2013), Global gravity field modeling based on GOCE and complementary gravity data, *Int. J. Appl. Earth Obs.*, *35*, 120–127, doi:10.1016/j.jag.2013.10.005.
Filmer, M. S. (2014), Using models of the ocean's mean dynamic topography to identify errors in coastal geodetic levelling, *Mar. Geod.*, *37*, 47–64, doi:10.1080/01490419.2013.868383.
Fischer, I. (1977), Mean sea level and the marine geoid—An analysis of concepts, *Mar. Geod.*, *1*(1), 37–59, doi:10.1080/01490417709387950.
Griesel, A., M. R. Mazloff, and S. T. Gille (2012), Mean dynamic topography in the Southern Ocean: Evaluating Antarctic Circumpolar Current transport, *J. Geophys. Res.*, *117*, C01020, doi:10.1029/2011JC007573.
Higginson, S., K. R. Thompson, J. Huang, M. Véronneau, and D. G. Wright (2011), The mean surface circulation of the North Atlantic subpolar gyre: A comparison of estimates derived from new gravity and oceanographic measurements, *J. Geophys. Res.*, *116*, C08016, doi:10.1029/2010JC006877.
Hirt, C., S. Claessens, T. Fecher, M. Kuhn, R. Pail, and M. Rexer (2013), New ultrahigh-resolution picture of Earth's gravity field, *Geophys. Res. Lett.*, *40*, 4279–4283, doi:10.1002/grl.50838.
Huang, J., and M. Veronneau (2013), Canadian gravimetric geoid model 2010, *J. Geod.*, *87*, 771–790, doi:10.1007/s00190-013-0645-0.
Huthnance, J. (1992), Extensive slope currents and the ocean-shelf boundary, *Prog. Oceanogr.*, *29*(2), 161–196, doi:10.1016/0079-6611(92)90023-S.
Huthnance, J. M. (2004), Ocean-to-shelf signal transmission: A parameter study, *J. Geophys. Res.*, *109*, C12029, doi:10.1029/2004JC002358.
Jain, A. K. (2010), Data clustering: 50 years beyond *K*-means, *Pattern Recogn. Lett.*, *31*(8), 651–666, doi:10.1016/j.patrec.2009.09.011.
Leaman, K., R. Molinari, and P. Vertes (1987), Structure and variability of the Florida Current at 27°N: April 1982 to July 1984, *J. Phys. Oceanogr.*, *17*, 565–583.
Lentz, S. J. (2008), Observations and a model of the mean circulation over the middle Atlantic bight continental shelf, *J. Phys. Oceanogr.*, *38*(6), 1203–1221, doi:10.1175/2007JPO3768.1.
Marsh, R., B. A. de Cuevas, A. C. Coward, J. Jacquin, J. J.-M. Hirschi, Y. Aksenov, A. G. Nurser, and S. A. Josey (2009), Recent changes in the North Atlantic circulation simulated with eddy-permitting and eddy-resolving ocean models, *Ocean Model.*, *28*(4), 226–239, doi:10.1016/j.ocemod.2009.02.007.
Menemenlis, D., J.-M. Campin, P. Heimbach, C. Hill, T. Lee, A. Nguyen, M. Schodlok, and H. Zhang (2008), ECCO2: High resolution global ocean and sea ice data synthesis, *Mercator Ocean Q. Newslett.*, *31*, 13–21.
Middleton, J. H. (1987), Steady coastal circulation due to oceanic alongshore pressure gradients, *J. Phys. Oceanogr.*, *17*(5), 604–612, doi:10.1175/1520-0485(1987)017.
Montgomery, R. (1938), Fluctuations in monthly sea level on eastern U.S. Coast as related to dynamics of western North Atlantic Ocean, *J. Mar. Res.*, *1*, 165–185.
Pavlis, N. K., S. A. Holmes, S. C. Kenyon, and J. K. Factor (2012), The development and evaluation of the Earth Gravitational Model 2008 (EGM2008), *J. Geophys. Res.*, *117*, B04406, doi:10.1029/2011JB008916.
Pearson, C., and R. Snay (2013), Introducing HTDP 3.1 to transform coordinates across time and spatial reference frames, *GPS Solut.*, *17*(1), 1–15, doi:10.1007/s10291-012-0255-y.
Penna, N., W. Featherstone, J. Creteaux, and R. Bingham (2013), The apparent British sea slope is caused by systematic errors in the levelling-based vertical datum, *Geophys. J. Int.*, *194*, 772–786.
Rossby, T., C. N. Flagg, K. Donohue, A. Sanchez-Franks, and J. Lillibridge (2014), On the long-term stability of Gulf Stream transport based on 20 years of direct measurements, *Geophys. Res. Lett.*, *41*, 114–120, doi:10.1002/2013GL058636.
Sallenger, A. H., K. S. Doran, and P. A. Howd (2012), Hotspot of accelerated sea-level rise on the Atlantic coast of North America, *Nature Clim. Change*, *2*, 884–888, doi:10.1038/nclimate1597.
Scott, J. T., and G. T. Csanady (1976), Nearshore currents off Long Island, *J. Geophys. Res.*, *81*(30), 5401–5409, doi:10.1029/JC081i030p05401.
Sturges, W. (1974), Sea level slope along continental boundaries, *J. Geophys. Res.*, *79*(6), 825–830.
Sturges, W. (1977), Comment on 'nearshore currents off Long Island' by J. T. Scott and G. T. Csanady, *J. Geophys. Res.*, *82*(9), 1451–1452, doi:10.1029/JC082i009p01451.
Tibshirani, R., G. Walther, and T. Hastie (2001), Estimating the number of clusters in a data set via the gap statistic, *J. R. Stat. Soc. B Met.*, *63*(2), 411–423, doi:10.1111/1467-9868.00293.
Woodworth, P., and R. Player (2003), The permanent service for mean sea level: An update to the 21st century, *J. Coast. Res.*, *19*, 287–295.
Woodworth, P., C. Hughes, R. Bingham, and T. Gruber (2012), Towards worldwide height system unification using ocean information, *J. Geod. Sci.*, *2*, 302–318, doi:10.2478/v10156-012-0004-8.

Wright, D. (1986), On quasi-steady shelf circulation driven by along-shelf wind stress and open-ocean pressure gradients, *J. Phys. Oceanogr.*, *16*, 1712–1714.

Xu, F.-H., and L.-Y. Oey (2011), The origin of along-shelf pressure gradient in the Middle Atlantic Bight, *J. Phys. Oceanogr.*, *41*(9), 1720–1740, doi:10.1175/2011JPO4589.1.

Yin, J., and P. B. Goddard (2013), Oceanic control of sea level rise patterns along the East Coast of the United States, *Geophys. Res. Lett.*, *40*(20), 5514–5520, doi:10.1002/2013GL057992.

Auxillary material for

The tilt of mean sea level along the east coast of North America

S. Higginson

(Bedford Institute of Oceanography, Dartmouth NS, Canada)

K.R. Thompson

(Department of Oceanography, Dalhousie University, Halifax NS, Canada)

P.L. Woodworth

(National Oceanography Centre, Liverpool, UK)

C.W. Hughes

(National Oceanography Centre, Liverpool, UK and
School of Environmental Sciences, University of Liverpool, Liverpool, UK)

Geophysical Research Letters, 2015

Introduction

This dataset contains eighteen estimates of ocean mean dynamic topography (MDT) at eleven coastal tide gauge locations, used to produce Figures 1 and 2. Seven of the estimates are derived from tide gauge measurements and geoid models, and the other eleven estimates are derived from ocean circulation models, as described in detail in the paper. The estimates are adjusted to relate to the time period 1996 to 2000. For each of the eighteen estimates, the mean MDT for that estimate has been subtracted from the MDT at each of the tide gauges. The MDT estimates are in table “ts01.txt”.

ts01.txt

Eighteen MDT estimates at eleven coastal tide gauge locations, used to produce Figures 1 and 2.

Column 1: Latitude (degrees latitude)
Column 2: Longitude (degrees longitude east of Greenwich)
Column 3: MDT (metres) estimated from the ECCO2 ocean model (reference O1 in the paper)
Column 4: MDT (metres) estimated from the OCCAM ocean model (reference O2)
Column 5: MDT (metres) estimated from the Liverpool ocean model (reference O3)
Column 6: MDT (metres) estimated from the NOC ORCA12 ocean model (reference O4)
Column 7: MDT (metres) estimated from the HYCOM ocean model (reference O5)
Column 8: MDT (metres) estimated from the HYCOM ocean model (reference O6)

Column 9: MDT (metres) estimated from the Mercator ocean model (reference O7)
Column 10: MDT (metres) estimated from the Glorys2v3 ocean model (reference O8)
Column 11: MDT (metres) estimated from the UR025 ocean model (reference O9)
Column 12: MDT (metres) estimated from the CGLORS ocean model (reference O10)
Column 13: MDT (metres) estimated from the MJM105b ocean model (reference O11)
Column 14: MDT (metres) estimated from the CGG2013 geoid model (reference G1)
Column 15: MDT (metres) estimated from the EGM2008 geoid model (reference G2)
Column 16: MDT (metres) estimated from the GOCO03S geoid model (reference G3)
Column 17: MDT (metres) estimated from the USGG2012 geoid model (reference G4)
Column 18: MDT (metres) estimated from the GGMplus geoid model (reference G5)
Column 19: MDT (metres) estimated from the TUM2013C geoid model (reference G6)
Column 20: MDT (metres) estimated from the GOCO03S extended geoid model (reference G7)

44.6611000000000 -63.5867000000000 -0.0462264222177592 -0.0477895826859907 -0.130622788450935
-0.000641583529385511 -0.0272310935178219 -0.0519872650948306 -0.0160397611070747
-0.0553419656049686 -0.0375025394965302 -0.0832954016025200 -0.0196302571552664
-0.0690189412133387 -0.0624156785590638 0.0359425594828464 -0.0874530224860641
-0.0970078515840921 -0.0798139165611454 -0.0914095863042458
43.6567000000000 -70.2467000000000 -0.0727132064375010 -0.0838836531205611 -0.161871334097602
-0.0302009249600496 -0.0705694372568614 -0.0842666898242768 -0.0583442943976106
-0.0988470039259868 -0.0730567607689988 -0.111624395022326 -0.0558255753077736
-0.0831477757133379 -0.101983201672064 -0.162072412242155 -0.0985596759860647
-0.0272208258140910 -0.115029843419047 -0.0883452018042457
41.5050000000000 -71.3267000000000 -0.0692305666479197 -0.0988783659501509 -0.146106525442817
-0.0272792178067293 -0.0569645395600236 -0.0962072103727434 -0.0490455593976010
-0.0966414314003267 -0.0781636276254149 -0.105550764669511 -0.0603245279349556
-0.0887467978133346 -0.100023569752062 0.0771580740898498 -0.0951486440860604
-0.124675939198387 -0.0902655466341416 -0.0969745479042433
40.7000000000000 -74.0133000000000 -0.0617267889055339 -0.113065080122514 -0.164334829828956
-0.0373258028897373 -0.0555677670952386 -0.0677897451772798 -0.0428182497832082
-0.104181385188448 -0.0722722801972519 -0.105081556905839 -0.0758028264997075
-0.0312097853066634 -0.0244628144533944 -0.104952882267481 -0.0246883515793903
-0.0590792457703205 -0.0722228342582718 -0.0595903573975721
39.3550000000000 -74.4183000000000 -0.0591482025655833 -0.103316544966264 -0.146257027170875
-0.0312721529873936 -0.0724831824785329 -0.0940095175064797 -0.0445842580835863
-0.104791688570527 -0.0770283836532723 -0.109278547683888 -0.0797477840043774
-0.0872856039733266 -0.116344366626053 -0.0980371580971474 -0.132055018246054
-0.125988024533683 -0.0467797705944358 -0.0252571820642347
36.1833000000000 -75.7467000000000 -0.0251237553629008 -0.0874855207963424 -0.102877636931159
-0.0176616488370028 -0.0550596980672112 -0.106814258072673 -0.0711226915545419
-0.108137400099782 -0.0808977498023799 -0.110585532505844 -0.0762579064724516
-0.0485446357333346 -0.0126374094590612 -0.413268416332157 -0.0184685860060631
-0.0504162584798923 -0.0379164705541464 -0.0506606698242439
33.6550000000000 -78.9183000000000 -0.0191227597269145 -0.0315573210282760 0.0472444929859855
-0.0463992892178623 -0.0181843485138341 0.0269505114615298 -0.0411618335638572
-0.0154986397913572 -0.0400021293172330 -0.0191969200169379 -0.0340546447691988
-0.0426258474866602 -0.0165451906783868 -0.271773236979483 -0.0208287977593903
0.0146058385291848 -0.0426036042061733 0.00882982142242642
32.0333000000000 -80.9017000000000 -0.00225780430165204 0.0118065019087358 0.0879248239777305
-0.0467591982754795 0.0178751968828200 0.0421003387521659 -0.0364575811652038
0.0326789824673060 -0.000191656590411166 0.0192213925401037 -0.00628713020758535
0.00294698184666359 -0.0191538893150646 0.107785085961846 0.0189795355739358
0.0551149893292117 0.0100425732023530 0.0374588927557537
28.4150000000000 -80.5917000000000 0.0165653723207387 0.0284244523481889 0.123369167067788
-0.0287102785977450 0.0208796488897419 0.0382969312066579 -0.00883073462267114
0.0826996860785805 0.0524061998070189 0.0776728924387113 0.0194697433553467
0.0383891605799973 0.0311802943932723 0.273650745208182 0.0453634283072711
0.0511845949363444 0.0623814587048925 0.0806313014890908
25.7300000000000 -80.1617000000000 0.143678416582671 0.236796907945113 0.253624872185967
0.0798400601473722 0.129417773132394 0.188124406503400 0.151835995609832 0.224618040699738
0.175213233353288 0.238832302147079 0.146475732335680 0.175487826453332
0.174156243172603 0.265829890714516 0.159283754180605 0.177190582873077 0.234088919749924
0.119075657362422
24.5550000000000 -81.8067000000000 0.195305717262355 0.288948206468062 0.339906785704873
0.186410036954013 0.187887447584568 0.205602498124529 0.216568968065523 0.243442805335772
0.231495694291185 0.308886531280972 0.241985176660290 0.233755418360003

0.248229582949274 0.289737750461184 0.253575378087275 0.186292139712648 0.178119034570192 0.166241872269093